Fluorocarbon Gas Exposure Induces Disaggregation of Nanodiamond Clusters and Enhanced Adsorption, Enabling Medical Microbubble Formation

Estefania Mendoza-Ortega, Marc Dubois, Marie Pierre Krafft

Fluorocarbon Gas Exposure Induces Disaggregation of Nanodiamond Clusters and Enhanced Adsorption, Enabling Medical Microbubble Formation

Estefania E. Mendoza-Ortega[1], Marc Dubois[2], and Marie Pierre Krafft[1]*

[1]University of Strasbourg. Institut Charles Sadron (CNRS). 23 rue du Loess. 67034 Strasbourg, France.

[2]Université Clermont Auvergne (UCA), CNRS, Sigma Clermont, ICCE, UMR 6296, 63178 Aubière, France

Corresponding Author* E-mail: **krafft@unistra.fr**

ORCID: ID: orcid.org/0000-0002-3379-2783

ABSTRACT

Introducing fluorocarbon vapor in the air above an aqueous dispersion of clusters of nanodiamonds induces their disaggregation, a prerequisite for most of their biomedical uses. Furthermore, the fluorocarbon gas promotes the adsorption of nanodiamonds at the gas/water interface. As an example of the benefits that can be gained from our findings relative to the implementation of nanomaterials for practical uses, we investigated the role that a fluorocarbon gas may play in the generation of microbubbles, which are currently actively investigated in ultrasound-mediated diagnosis and therapy. Remarkably, the fluorocarbon gas enables the production of microbubbles shelled only with nanodiamonds, in the absence of any other surfactant, which could not be achieved without the fluorocarbon being present. This demonstrates that a supernatant gas can decisively affect the adsorption of nanoparticles from an aqueous phase to an air/water interface, likely through physical adsorption at the nanodiamond surface. The investigations involved solid-state NMR and FTIR, microbubble generation experiments with acoustic attenuation monitoring, and bubble profile analysis tensiometry on spontaneously adsorbed Gibbs films. Perspectives include control of aggregation of nanodiamonds and their retrieval from aqueous dispersions, and applications in multimodal diagnostic imaging, bioimaging and therapeutic cell tracking. It is proposed that the disaggregating potency of fluorocarbons can be applied to other nanomaterials, providing a simple and effective means of alleviating aggregation.

GRAPHICAL TABLE OF CONTENT
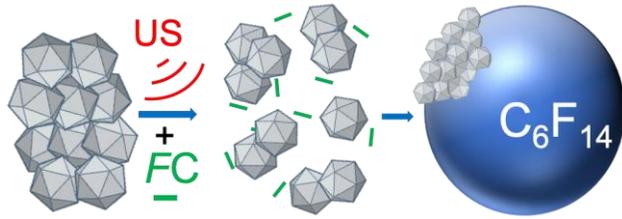
Exposing aqueous dispersion of nanodiamonds to fluorocarbon vapor disaggregates clusters and allows recruitment of the nanoparticles at the air/gas interface. This effect is stronger with fluorinated nanodiamonds. This new gas-driven phenomenon allowed preparation of nanodiamond-shelled microbubbles for potential use in bioimaging, cell tracking and ultrasound-mediated diagnostic and therapy.

INTRODUCTION

Nanodiamonds (NDs) capture considerable attention in various fields, from electronics and optics to biomedicine, due to a range of specific properties, such as high refractive index and scattering efficiency, outstanding mechanical performance (*e.g.* super-hardness), and versatile surface chemistry and biocompatibility.[1-4] In biology and medicine, they are actively investigated for sensing, bioimaging and drug delivery.[5-7] In particular, fluorescent NDs are being investigated as a less-toxic alternative to semiconductor quantum dots (QDs).[8] NDs can be surface-conjugated with many biologically active molecules and targeting ligands using covalent or non-covalent (*e.g.* electrostatic or hydrophobic) interactions.[4] However, most biomedical applications of NDs are still impeded due to their strong tendency for aggregation when dispersed in an aqueous phase. Various techniques of ND disaggregation, crushing and fractionation have been reviewed,[9] including zirconia microbead-assisted wet ball milling,[10] salt (or sugar)-assisted dry attrition and ball milling,[11] and bead-assisted sonic disintegration[12-14] Although these techniques proved efficient, and produced colloidal dispersions of nanodiamonds with particles lower than 10 nm,[11] the risk of contamination, either by metal ions or ceramic debris, remained, and made mandatory additional purification steps, reducing the overall efficiency and increasing the cost. A salt-assisted ultrasonic disaggregation process that is based on sonication of aqueous NaCl/ND slurries followed by washing/centrifugation steps was also effective.[15] Although the authors claimed the absence of contamination, a long sonication time (over 1 h) using a titanium tip is well-known to produce metal contamination by erosion of the probe due to the high intensity cavitation energy.[16] Functionalization of NDs with zwitterionic moieties,[17] or adsorption of polyelectrolytes,[18] or amino acids[19] improved the dispersibility of NDs. Various methods of ND encapsulation, as in

1 phospholipid liposomes,[20] or in silica[21] or dopamine[22] shells have also been reported. Control of

2 ND aggregation in aqueous solutions through simple approaches is therefore sought for.

3   We propose here a simple mean to induce dispersion of NDs in aqueous solutions that does not

4 involve chemical modification of the NDs, which consists in exposing ND dispersions to vapor of

5 a fluorocarbon (FC). We show that the capacity for a FC gas to recruit NDs to a gas/water interface

6 also unlocks the possibility to prepare microbubbles (MBs), which, to our knowledge, is

7 impossible in the absence of the FC. Microbubbles are used in the clinics as ultrasound contrast

8 agents, and their efficacy as mediators in ultrasound therapy is actively investigated.[23-28] Medical

9 microbubbles, especially those stabilized by a phospholipid shell, are often stabilized by a

10 fluorocarbon gas. It is noteworthy that fluorocarbons are chemically and biologically inert, due to

11 the strength of the C-F bond. A variety of nanoparticles (NPs), including gold, magnetic iron oxide

12 or CdTe QDs, can be attached to MBs, or form the bubble shell, in order to extend the range of

13 their uses, as for combining multimodal imaging procedures, targeted drug delivery or therapeutic

14 energy deposition.[29-30] Despite increasing interest for NP-coated microbubbles, MBs with a shell

15 of nanodiamonds have never been reported. Controlling nanoparticle adsorption and behavior at

16 interfaces is key to achieving versatile ultrasound imaging and theranostic agents.

17   We have previously shown that perfluorohexane (F-hexane) vapor substantially accelerates the

18 adsorption at a gas/water interface of a variety of molecules, including fluorinated biomarkers,[31]

19 proteins[32] and block copolymers[33], helps control their self-assembly at the interface and promote

20 efficient stabilization of MBs. Also relevant to this work, we found in a previous report that

21 exposure to F-hexane can disaggregate protein Hydrophobin HFBII.[32] We thus questioned whether

22 FC-induced adsorption would occur with nanoparticles tens of nanometers in size, and whether

23 such enhanced adsorption could ensure stabilization of MBs that would be shelled solely by these

1   NPs. It should be noted that, although the parameters that condition the adsorption of NPs at fluid

2   interfaces have been investigated,[34] the potential effect of the nature of the supernatant gas phase

3   has, to our knowledge, never been considered. Here, we report the capacity for FC gases to

4   disaggregate ND clusters, recruit NDs at the air/water interface, and form MB shells. This

5   investigation was achieved with fluorinated and non-fluorinated NDs in the presence, or absence,

6   of FC gases (Scheme 1).

7   **Scheme 1.** Schematic representation of aqueous dispersions of nanodiamonds (ND25 or F-ND25)

8   exposed to air saturated with vapors of perfluoropentane or perfluorohexane.

9
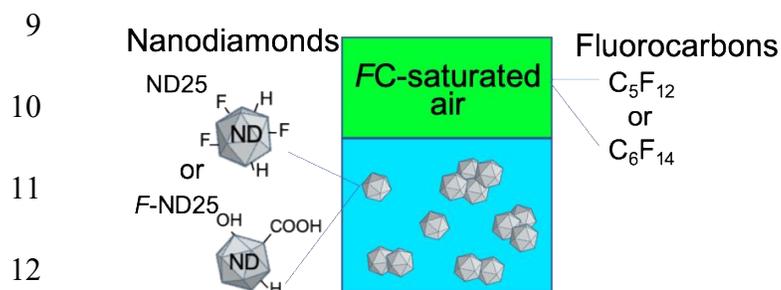
13 We found that 1) exposure to F-hexane or perfluoropentane (F-pentane) vapor readily induces

14 significant disaggregation of the clusters formed by both types of nanodiamonds in aqueous

15 dispersions; 2) the adsorption kinetics of both types of NDs at a gas/water interface is markedly

16 impacted by exposure to the FC, both in terms of rate and interfacial tension lowering, and 3)

17 microbubbles (~2-4 µm in average diameter) can be produced from both types of NDs as sole shell

18 components when, and only when, F-hexane is introduced in the gas phase.

19 **EXPERIMENTAL SECTION**

20 **Materials and Methods.** Nanodiamonds (ND25, 25 nm in diameter, Tomei Diamond Co,

21 Tokyo, Japan) were prepared by size separation of powdered bulk diamond synthesized using a

22 static high-pressure high-temperature (HPHT) method. They were subsequently treated with heated

23 solutions of acids to remove impurities and characterized following previous reports.[35-36]

1   Fluorinated analogs of ND25 (*F*-ND25) were obtained from the same commercial batch by direct

2   fluorination of ND25 with difluorine (F_2, 1 atm, 500°C, 12 h).[35-36] Perfluorohexane (*F*-hexane, 98%)

3   and perfluoropentane (*F*-pentane, 98%) were purchased from Fluorochem (UK). Water was

4   obtained from a Milli-Q (Millipore) system (surface tension: 71.7 ± 0.2 mN m^{-1} at 20 °C; resistivity:

5   18.2 MΩ cm). FTIR experiments were performed on a Vertex 70 (Bruker) spectrometer. Solid state

6   NMR experiments were performed on a Tecmag spectrometer (Tecmag Inc., Houston, TX) with

7   operating frequencies of 500.33, 470.74 and 125.81 MHz for ^{1}H, ^{19}F and ^{13}C, respectively. A simple

8   sequence (τ-acquisition) was used with a single $\pi/2$ pulse length of 3.5 µs for ^{1}H and ^{13}C nuclei and

9   a recycle time of 3 and 5 s. For ^{19}F MAS spectra, the $\pi/2$ pulse duration was 5.5 µs and the recycle

10   time was 5 s. ^{19}F chemical shifts were referenced to $CFCl_3$, and tetramethylsilane (TMS) was the

11   reference for both ^{1}H and ^{13}C chemical shifts. The contact angles of water droplets (3-10 µL)

12   deposited on the surface of pellets of nanodiamonds (obtained under a pressure of 0.2 ton; 5 mm in

13   diameter) were measured using an Attension Theta Lite Optical Tensiometer with an imaging source

14   camera. The measurements were repeated 3 times at different pellet locations in a temperature-

15   controlled room (19°C) with constant relative humidity (33%).

16   **Preparation of Aqueous Dispersions of Nanodiamonds (NDs) Exposed to Air or to a**

17   **Fluorocarbon gas.** ND25 and *F*-ND 25 were dispersed in MilliQ water (2 mL) at room temperature

18   and sonicated in an ultrasound bath (UCS 300T, 45 kHz, 80 W, 2.8 L, VWR) for 10 min at 25°C.

19   Concentrations were 0.05 g L^{-1} for the DLS measurements (2 mL) and 0.1 g L^{-1} for the tensiometry

20   (6 mL), cryogenic transmission electron microscopy (cryo-TEM) and microbubble experiments (1

21   mL). The pH of the ND aqueous dispersions was adjusted to 12 using a NaOH solution (1 M) in

22   order to allow ionization of the acid functions present on the ND surface, after which the dispersions

23   were sonicated in the sonication bath for another 20 min. Aliquots for analysis by DLS and

1 tensiometry, and for the preparation and characterization of microbubbles, were placed into the

2 appropriate measuring cells. For the experiments conducted under fluorocarbon exposure (F-hexane

3 or F-pentane), N_2 was allowed to bubble through three successive vials containing the fluorocarbon

4 (more details are provided in [37]) prior to being flushed for 10 min into the measuring cells used in

5 DLS, tensiometry and microbubble preparation. For comparison, sonication was also achieved using

6 a tip sonicator (Vibracell, Bioblock Scientific, Illkirch, France) equipped with a 3 mm titanium

7 probe (setting 5, duty cycle 40%) and operated at 20 kHz.

8 **Dynamic Light Scattering and Zeta Potential.** The ND aqueous dispersions (0.05 g L^{-1}) were

9 prepared as described above and filtered on 0.22 µm filters (Millex-GP PES 33 mm Millipore).

10 They were either exposed to air or to F-hexane- (or F-pentane)-saturated air in capped cylindrical

11 glass cuvettes (outer diam.: 10 mm, l: 75 mm, Hellma Analytics). The size distributions of the

12 nanodiamond clusters in aqueous dispersions were measured using an experimental set-up (ALV

13 GmbH, Langen, Germany) equipped with a He-Ne laser (22 mW, $\lambda_0 = 632.8$ nm), a compact ALV

14 CGS-8 goniometer and an ALV-7002 autocorrelator. The samples were analyzed at 90°, after

15 preparation, after treatment in the sonication bath and after 2 days at room temperature. The

16 autocorrelation functions were based on 60 runs with 60 s counting time. The data were analyzed

17 using the CONTIN algorithm,[38] which allows determination of the mean hydrodynamic radius r_h

18 and polydispersity index (PDI). PDI values varied from 13 to 22%. Zeta potential was measured

19 after preparation with a Zetasizer Nano ZS (Malvern Panalytical, Grovewood Road, Malvern,

20 UK). It was deduced from the electrophoresis mobility using the Henry equation: $U_E =$

21 $2\varepsilon\zeta f(K_a)/3\eta$, U_E being the electrophoretic mobility, ε the dielectric constant, ζ the zeta potential,

22 $f(K_a)$ the Henry function and η the viscosity of the medium. The results are the average of 3 runs

23 with 100 s counting time and they were repeated 3 times (error was $\pm$ 1 mV).

Cryogenic Transmission Electron Microscopy of Aqueous Dispersions of Nanodiamonds.
Cryo-TEM experiments were performed with a FEI Tecnai G2 electron microscope (operating at 200 kV) under low dose conditions with an Eagle slow scan CCD camera. A laboratory-built humidity and temperature-controlled vitrification system was used to prepare the samples. Humidity was kept close to 80% for all experiments and the temperature was set at 22°C. 5 µL aliquots of the ND dispersions (0.1 g L^{-1}) were placed onto a grid covered by a lacey carbon film (Ted Pella, Redding, United States) that serves as an electron transparent support. This grid was rendered hydrophilic using a Glow 2 discharge system (Elmo, Cordouan Technologies, Bordeaux, France). Excess solution was removed by blotting with filter paper, and the sample grid was vitrified by rapid plunging into liquid ethane. The grids were kept in liquid nitrogen before being transferred into a Gatan 626 cryo-holder.

Preparation and Observation of Nanodiamond-Shelled Microbubbles by Optical Microscopy. A 1 mL aliquot of the ND dispersions (0.1 g L^{-1}) was transferred to a cylindrical glass tube (outer diameter: 10 mm, length: 25 mm) and subjected to agitation/amalgamation using a Vialmix® (2 cycles of 45 s, Lantheus Medical Imaging N. Billerica, MA) at room temperature. The samples were observed using a Nikon Eclipse 90i microscope (Nikon Instruments Europe, Amsterdam, The Netherlands). One 8 µl droplet was placed into a concave slide and covered with a glass slide. Bubble mean diameter and distribution width were determined on 5−10 slides using *Fiji* (an open-source image processing package[39]) and the standard deviations using Origin9 (OriginLab Corp. Northampton, MA, USA).

**Echogenicity and Acoustical Determination of the Nanodiamond-Shelled Microbubble Size Distribution and Half-Life.** Our method is based on the attenuation, that is, the reduction in amplitude, of an acoustical wave that propagates through an aqueous dispersion of bubbles. A

1   method was developed that fits standard simple-harmonic resonator curves to measured

2   attenuations to infer the size of the bubbles.[40] A low-power emitter was used to avoid altering

3   bubble characteristics and stability (acoustical power: 0.1 W cm^{-2}; peak-to-peak acoustical

4   pressure $<3 \times 10^4$ Pa). More experimental details can be found in[37]. An aliquot of the ND-shelled

5   microbubbles (1 mL, ND concentration: 0.1 g L^{-1}) was injected in the ultrasonic measuring cell

6   (cell volume 140 mL) and thermoregulated at 25° C. The mean diameter of the microbubbles was

7   measured immediately after preparation and over time.

8   **Adsorption kinetics of nanodiamonds at the air/water interface (Bubble profile analysis**

9   **tensiometry).** Axisymmetric bubble shape analysis was applied to a rising gas bubble (7 µL)

10   formed in aqueous dispersions of nanodiamonds. Time dependence of σ during adsorption at the

11   gas/liquid interface was measured using a Tracker® tensiometer (Teclis Scientific, Lyon, France).

12   For the experiments achieved in the presence of *F*-hexane or *F*-pentane, a 100 µL syringe was

13   purged 10 times with the fluorocarbon-saturated air that surmounts liquid fluorocarbon according

14   to the protocol provided in [39]. At 25°C, *F*-hexane saturated vapor pressure and concentration at

15   25°C are 2.9 10^4 Pa and 11.66 mol m^{-3}, respectively; water solubility is 2.7 10^{-4} mol m^{-3}; *F*-pentane

16   saturated vapor pressure and concentration are 8.5 10^4 Pa and 34.14 mol m^{-3}, respectively; water

17   solubility is 4 10^{-3} mol m^{-3}).[41] The bubbles were formed in rectangular cuvettes (40 mm x 23.6

18   mm x 15 mm, Hellma Analytics) containing the ND aqueous dispersions (0.1 g L^{-1}). All

19   measurements were achieved at 24 ± 1 °C and repeated three to five times. The characteristic time

20   of adsorption τ was determined by fitting the adsorption profiles with an exponential decay

21   function.

22   **RESULTS AND DISCUSSION**

1   **Characterization of Nanodiamonds.** Commercial nanodiamonds (ND25, 25 nm in diameter),

2   prepared by size separation of powdered bulk diamond synthesized using a static high-pressure

3   high-temperature (HPHT) method were treated with heated solutions of acids to remove impurities

4   and were characterized according to[35-36]. Advantages of HPHT NDs over detonation NDs include

5   a substantially lower nitrogen content, which makes them better suited for fluorescent imaging

6   applications.[3] ND25 have a crystalline sp^3 carbon core and their surface is covered with an

7   amorphous sp^2 carbon shell displaying functional surface groups, mainly CH, COH, CO and

8   COOH.[35-36] Fluorinated analogs of ND25 (*F*-ND25) were obtained from the same commercial

9   batch by direct fluorination of ND25 with difluorine (F_2, 1 atm, 500°C, 12 h).[36] Fluorination

10   drastically changes the surface chemistry of ND25, as indicated by FTIR spectra (Figure 1) that

11   show the appearance of C-F stretching vibrations (1100-1400 cm^{-1}); disappearance of the broad

12   band of OH stretching (3280-3675 cm^{-1}) and bending (1640 cm^{-1}) vibrations; replacement of the

13   bands at 1700-1870 cm^{-1}, attributed to C=O, by C-F bands; the C-H bands (2900 cm^{-1}) are partly

14   maintained and more resolved for the fluorinated NDs. These observations are confirmed by multi-
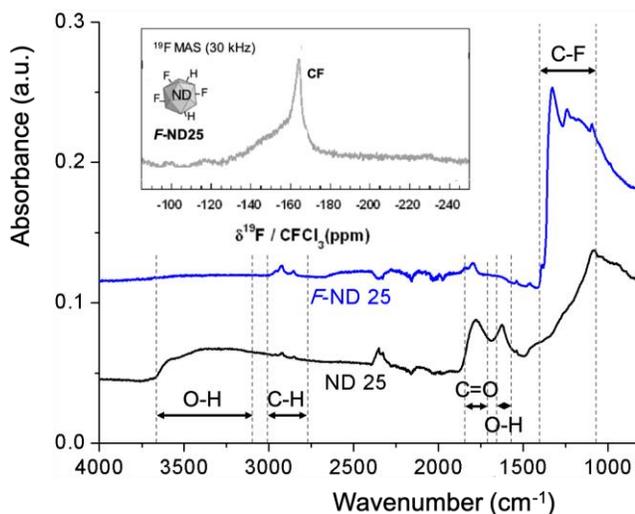
23   **Figure 1.** FTIR spectra of ND25 and *F*-ND25 nanodiamonds. Inset: ^{19}F MAS NMR spectrum of

24   *F*-ND25 showing C-F bonds at -170 ppm.

1   nuclear solid-state NMR. The $^1H\rightarrow^{13}C$ CP-MAS spectrum confirms the presence of COOH (160

2   ppm), COH (75 ppm), CH (45 ppm) groups, of sp^3 C (35 ppm) and of a low content of sp^2 C

3   (amorphous C shell on ND surface, 120 ppm) (SI, Figure S1a). In the ^1H MAS spectrum recorded

4   after fluorination, only C-H band (at 1.5 ppm) is observed and no more C-OH (SI, Figure S1b).

5   The ^{19}F MAS spectrum reveals the presence of covalent C-F bonds with a chemical shift of -170

6   ppm (inset in Figure 1).

7   The contact angles of a droplet of water deposited on the surface of pellets formed by the NDs

8   under pressure were measured. These contact angles are only "apparent", because of the roughness

9   of the pellets. Nevertheless, the method provided evidence of significant differences in surface

10   chemistries between non-fluorinated and fluorinated nanodiamonds. The contact angle was 130° in

11   the case of *F*-ND25, reflecting the hydrophobic character of the *F*-ND25 pellet surface. By contrast,

12   the water droplets were readily absorbed into the pellets of ND25, preventing any measurement but

13   confirming the hydrophilic character of the ND25 surface.

14   **Effect of Fluorocarbon Gases on Nanodiamond Disaggregation in Aqueous Solutions.** We

15   studied the effect of exposing aqueous dispersions of ND25 and *F*-ND25 to *F*-hexane and *F*-

16   pentane vapors. An essential requirement for the development of any biological application is

17   indeed to be able to obtain stable, minimally aggregated, reproducible aqueous ND dispersions,

18   which depends on various parameters, including the surface potential of the particles, pH,

19   temperature and concentration.[42] Aqueous dispersions of ND25 and *F*-ND25 (0.05 g L^{-1}) were

20   prepared in Milli-Q water at room temperature and pH was adjusted to 12.0 in order to allow

21   ionization of the carboxylic acid functions in the case of ND25, and provide similar ionic

22   environment in the case of *F*-ND25. The mean hydrodynamic radius r_h of the ND clusters was

23   determined by dynamic light scattering (DLS) after filtration of the dispersions on 0.22 µm filters.

1   The zeta potential ζ of the dispersions was measured under air and under F-hexane- (or F-pentane)

2   saturated air after preparation. We achieved a study to compare the effects of bath sonication versus

3   tip sonication, as an attempt to disaggregate the ND clusters in aqueous dispersions. We

4   systematically found larger clusters in the case of tip sonication. For example, under air, ND25

5   clusters with r_h of 69 ± 2 nm were obtained after 2 min of tip sonication. Increasing sonication

6   time only resulted in an increase of r_h to 112 ± 24 nm and 157 ± 31 nm after 5 and 10 min of

7   sonication, respectively. After 5 days of storage at 25°C, the cluster sizes reached 220 nm. By

8   contrast, bath sonication led to smaller ND25 clusters (58 ± 4 nm) after preparation that grew up

9   to 151 ± 4 nm after 2-week storage at room temperature. Bath sonication was thus used in all the

10   experiments. The data are collected in Table 1 and Figure 2. For ND25, r_h was 58 ± 4 nm when

11   measured under air immediately after preparation (*i.e.* the clusters contain ~9 primary particles).

12   This value did not change significantly when subjecting the dispersions to ultrasound bath

13   treatment (25°C, 20 min). After 2 weeks of storage at room temperature, significant aggregation

14   occurred in the aqueous dispersions, leading to larger clusters with a mean radius of 151 ± 4 nm

15   (~163 primary particles). By contrast, exposing the ND25 dispersions to F-hexane, or F-pentane,

16   vapors drastically changed their aggregation behavior. After ultrasound bath treatment, r_h

17   *decreased* significantly from 62 ± 3 nm (~11 primary particles) to 35 ± 1 nm (~2 primary particles),

18   when exposed to F-hexane, and from 65 ± 2 nm (~13 primary particles) to 29 ± 1 nm (~1 primary

19   particles) when exposed to F-pentane (SI Figure S2). ζ decreased significantly from -58.2 mV (air)

20   to -61.1 mV, and to -62.3 mV for F-hexane and F-pentane, respectively. After two-week storage,

21   the NDs exposed to the FC gases had maintained their size (37 and 32 nm, respectively). Zeta

22   potentials were found unchanged after one week at 25°C. These results indicate that exposure to

1 *F*Cs promotes disaggregation of the ND25 clusters and prevents their re-aggregation of the NDs

2 over time.

3 **Table 1.** Mean hydrodynamic radius r_h and zeta potential ζ of dispersions of nanodiamonds

4 exposed to air, *F*-hexane or *F*-pentane. In parentheses, the number of primary particles contained

5 in the nanodiamond clusters.

6

ND	Gas phase	r_h Prep. (nm)	r_h Sonic bath (nm)	r_h Storage* (nm)	ζ Prep. ($\pm$ 1 mV)
ND25	Air	58 ± 4 (9)	57 ± 2 (8)	151 ± 4 (163)	-58.2
	F-hexane	62 ± 3 (11)	35 ± 1 (2)	37 ± 1 (2)	-61.1
	F-pentane	65 ± 2 (13)	29 ± 1 (1)	32 ± 2 (1)	-62.3
F-ND25	Air	81 ± 3 (25)	83 ± 3 (26)	146 ± 4 (147)	-48.1
	F-hexane	87 ± 2 (31)	89 ± 2 (32)	75 ± 1 (19)	-50.4
	F-pentane	88 ± 4 (32)	88 ± 3 (32)	74 ± 3 (19)	-51.2

7 *Two weeks at room temperature.

8 Where *F*-ND25 NDs are concerned, r_h was 81 ± 3 nm (~25 primary particles) under air after

9 preparation. This larger size relative to that of ND25 reflects the higher hydrophobicity of the

10 fluorinated NDs at the surface of which the polar functions have been replaced by C-F bonds, and

11 their higher tendency for aggregation in aqueous media. The less negative zeta potential of the *F*-

12 ND25 dispersions exposed to air (-48.8 mV vs. -58.2 mV for ND25) also reflects the substitution

13 of polar functions by fluorine atoms. When exposed to air for 2 weeks at room temperature,

14 pronounced aggregation was observed, leading to *F*-ND25 clusters reaching 146 ± 4 nm in size

15 (~147 primary particles). By contrast, exposure to *F*-hexane or *F*-pentane led to significant

16 disaggregation of the *F*-ND25 clusters (~75 nm, ~19 primary particles). Disaggregation was

17 noticeable after 2 days at 25°C, which means that the process is slow for *F*-ND25. Importantly,

18 ND aggregation did not recommence over time when the *F*C gas was present. Exposure to

19 fluorocarbon gases slightly decreases the zeta potential of *F*-NDs (from -48.1 to -50.4 and -51.2

20 for *F*-hexane and *F*-pentane, respectively). These values did not change after one week at 25°C.
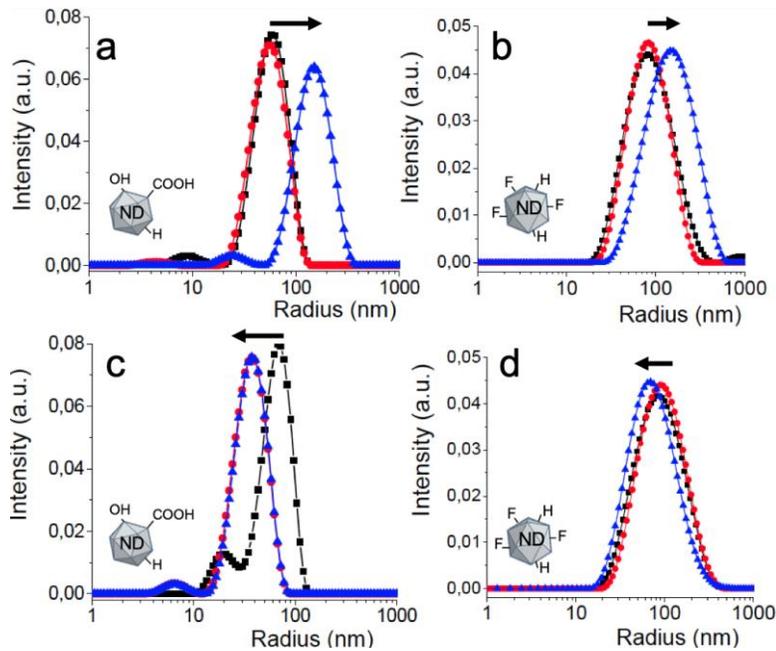
Figure 2. DLS profiles of ND25 (left panel) and *F*-ND25 (right panel) in aqueous dispersions (0.05 g L^{-1}) under air (a, b) and *F*-hexane-saturated air (c, d) showing the variation of intensity as a function of the hydrodynamic radius after preparation (black), after ultrasound bath treatment (red), and after two-week storage at room temperature (blue). In d), the difference between the values measured after preparation (87 ± 2 nm) and after storage (75 ± 1 nm) is significant. Arrows indicate the direction of peak radii variation.

The disaggregation effect of *F*-hexane on aqueous dispersions of NDs was also investigated by cryogenic transmission electron microscopy (cryo-TEM). Figure 3 shows that significant aggregation occurs in the aqueous dispersions of ND25 under air (3.a), while the aggregation is limited under *F*-hexane (3.b). More isolated primary particles that look transparent, as well as small aggregates can be observed (3.c-d), while only large aggregates are seen when the NDs are exposed to air.
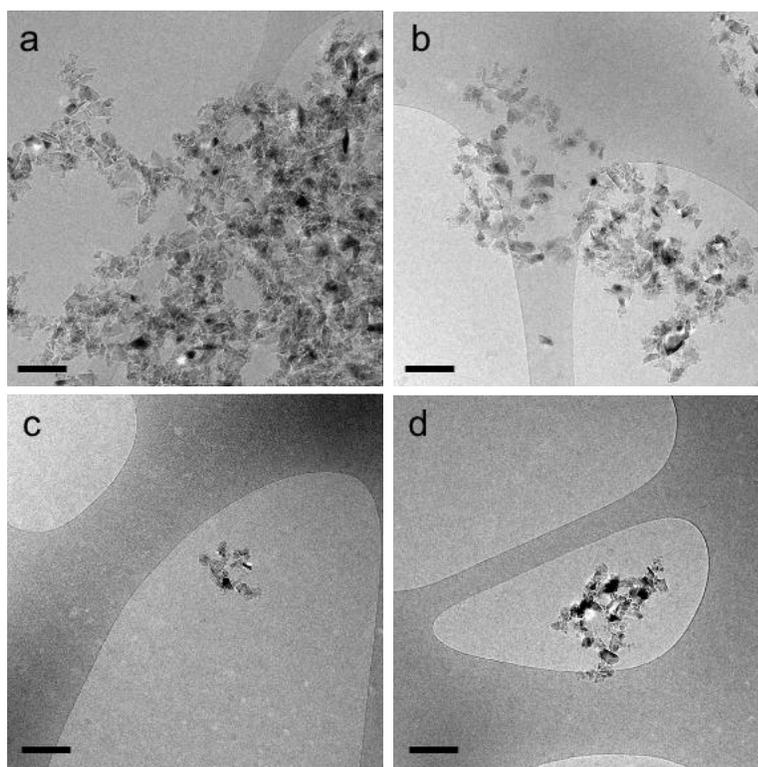
Figure 3. Cryo-TEM images of aqueous dispersions of ND25 (0.1 g L^{-1}) exposed a) under air and b) under *F*-hexane-saturated air (b-d). b-d) reveal the presence of relatively small isolated clusters that cannot be seen under air. Scale bar:100 nm.

One hypothesis for the mechanism of disaggregation and for the *F*C-induced improved ND dispersion stability is that, although the solubility of the *F*Cs in water is extremely low (2.7 x 10^{-4} mol m^{-3} and 4.0 x 10^{-3} mol m^{-3} for *F*-hexane and *F*-pentane, respectively, at 25°C)[41], it is not null. It can therefore be envisioned that *F*C molecules present in the aqueous phase interact with the clusters of NDs through hydrophobic interactions, which may break some of the interactions that ensure ND cluster cohesion, and induce their progressive disaggregation (Scheme 2). The more negative ζ values measured when both ND25 and *F*-ND25 are exposed to the *F*C gases support this view. Addition of surfactants was indeed shown to increase the colloidal stability of ND aqueous dispersions,[43] and the surface activity of *F*-hexane at interfaces has been established.[39]
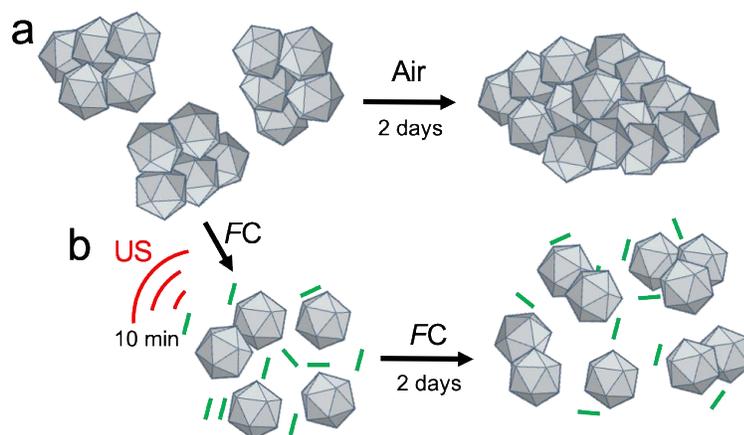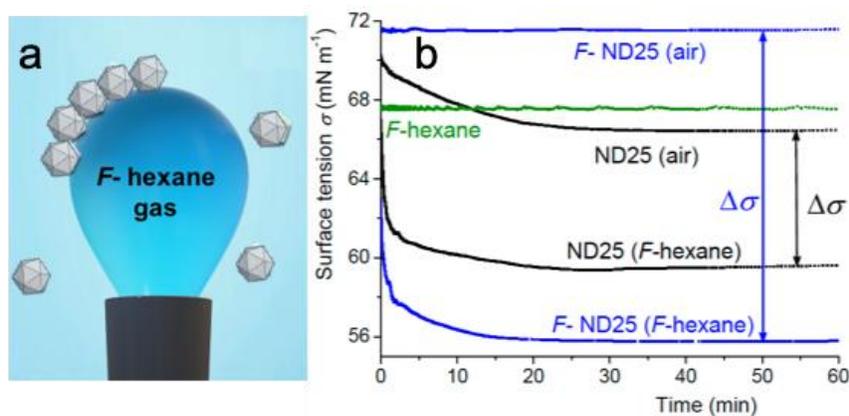
Scheme 2. Schematic representation of the aggregation of ND clusters that occurs under air over time (a), whilst disaggregation occurs under *F*-hexane (b) (green entities: *F*-hexane; not on scale).

The fact that the more water-soluble *F*-pentane is more efficient than *F*-hexane for ND25 cluster disaggregation also supports this view. The stronger disaggregating effect of the *F*C gas on non-fluorinated ND25 was unexpected. It may be possible that disaggregating *F*-ND25 clusters, which are larger than ND25 ones (they contain ~25 primary particles versus ~9), may require more fluorocarbon molecules, which is limited by the low water solubility of *F*-hexane and *F*-pentane. It may also be possible that *F*-NDs25 are more tightly packed.

Adsorption of Nanodiamonds at the Air/Water Interface. In order to shed light on the effect of the *F*C on MB formation, we determined the kinetics of the *F*-hexane-driven adsorption of ND25 and *F*-ND25 at the gas/water interface at 25°C using bubble profile analysis tensiometry. A syringe filled with *F*-hexane-saturated air was fitted on the measuring cell of the tensiometer.[39] The adsorption profiles of dispersions of ND25 and *F*-ND25 (0.1 g L^{-1}) exposed – or not – to *F*-hexane gas are provided in Figure 5. The characteristic time of adsorption τ was determined by fitting the adsorption profiles with an exponential decay function. Under air, ND25 adsorb only slightly and slowly ($\tau \sim 10.3$ min) at the interface. The equilibrium value of the interfacial tension

1 was reached after ~30 min (σ_{eq} ~66.4 mN m^{-1}). The weak adsorption of ND25 particles is explained

2 by their significant hydrophilic character, as measured by contact angle, due to the polar functions

3 present on the ND25 surface, and low affinity for the interface. Exposure of ND25 to *F*-hexane

4 results in a much faster (τ ~0.86 min) and more pronounced adsorption (σ_{eq} ~59.5 mN m^{-1}, *i.e.* a

5 σ lowering $\Delta\sigma$ = 6.9 mN m^{-1}). It should be reminded that *F*-hexane alone induces a lowering of

6 the tension of water of only 4.5 mN m^{-1} (Figure 5). This indicates a synergistic effect between *F*-

7 hexane and the NDs at the interface. By contrast with ND25, *F*-ND25 do not adsorb at all at the

8 interface under air, as assessed by a constant σ value of ~71.5 mN m^{-1}, which is probably due by

9 the large size of the clusters. By contrast, exposure to *F*-hexane leads to a pronounced adsorption,

10 causing a tension lowering $\Delta\sigma$ by ~15.8 mN m^{-1} with respect to the value measured in air. These

11 results suggest that fluorous interactions develop bet-

12

18 **Figure 5.** a) Schematic representation of the adsorption of nanodiamonds at the air/water interface
19 using bubble profile analysis tensiometry. b) Variation of the gas/water interfacial tension σ over
20 time for aqueous dispersions of ND25 (black) and *F*-ND25 (blue) under air and under *F*-hexane-
21 exposure (0.1 g L^{-1}, pH 12). Adsorption profile of *F*-hexane in the absence of nanodiamonds
22 (green). Concentration: 0.1 g L^{-1}; pH 12.0; temperature: 25°C.

-ween *F*-hexane and the fluorinated NDs, enabling the recruitment of the latter to the interface, and their stabilization at this interface. Although the interfacial behavior of spread films of nanodiamonds functionalized by alkyl (and fluoroalkyl) chains has been described,[44] our data are the first report of spontaneously adsorbed films of nanodiamonds at the gas/water interface.

To sum-up, the disaggregating effect exerted by the fluorocarbon both facilitates the diffusion of the nanodiamond particles to, and their organization at the interface, likely by filling the interparticle gaps. For *F*-NDs, these effects are enhanced, likely by fluorine-fluorine hydrophobic interactions that develop between the C-F groups and *F*-hexane, as was recently reported for magnetic nanoparticles fitted with dendrons terminated with fluorinated groups.[45]

Microbubbles with Nanodiamond Shells. In order to exploit the observed dispersive effect of *F*C gases on ND in aqueous dispersions, and influence of their adsorption at an air/water interface, we investigated the possibility of preparing microbubbles that would be shelled by NDs only, that is, without recourse to any conventional surfactant or foaming agent. Essentially all the commercially available medical microbubbles use *F*C gases for stabilization.[25-26] The latter acts as an osmotic agent and as a co-surfactant to the bubble shell-forming material (usually phospholipids).[23, 46] Preparation of MBs was attempted by bubbling either N_2 or *F*-hexane-saturated N_2 into aqueous dispersions of ND25 or *F*-ND25 (0.1 g L^{-1}). The MBs were prepared using a Vialmix® shaker in the presence, or absence, of *F*-hexane. Their size and stability characteristics were measured by optical microscopy and by an acoustical attenuation method.[40] We found that, for both ND25 and *F*-ND25, only the dispersions that were exposed to *F*-hexane did produce MBs stable enough for characterization. All our attempts to produce MBs in the absence of *F*C failed. The impossibility to generate MBs in the absence of *F*-hexane is strongly related to the interfacial behavior of nanodiamonds, as observed in tensiometry. For generating

1   MBs, it is crucial that the shell components access and stabilize the interface rapidly.[47] The

2   tensiometry experiments demonstrate that, under air, neither of the NDs are adsorbing at the

3   air/water interface in a significant manner. Under *F*-hexane exposure both types of nanodiamonds

4   are readily adsorbing at the interface, likely due to the fact that *F*-hexane fills in gaps left between

5   the nanodiamond particles, thus facilitating their organization in a compact film.

6   The *F*-ND25-shelled MBs were smaller and more narrowly dispersed (mean diameter: 2.14 ±

7   0.60 μm), than the ND25-shelled MBs (3.76 ± 0.89 μm) (Figure 3). The MBs made from ND25

8   and from *F*-ND25 were both highly echogenic. Their stability was determined by measuring the

9   attenuation coefficient α of ultrasound waves that propagate through a bubble dispersion as a

10 function of time for a range of ultrasound frequencies *f*. [40] The variation of α as a function of *f* at

11 the initial time t_0 (Figure 4a,b) shows that, for both types of NDs, the maximal value is comparable

12 to that of phospholipid-shelled MBs, suggesting comparable echogenicity for comparable volumes

13 of MBs injected in the measuring cell.[40]
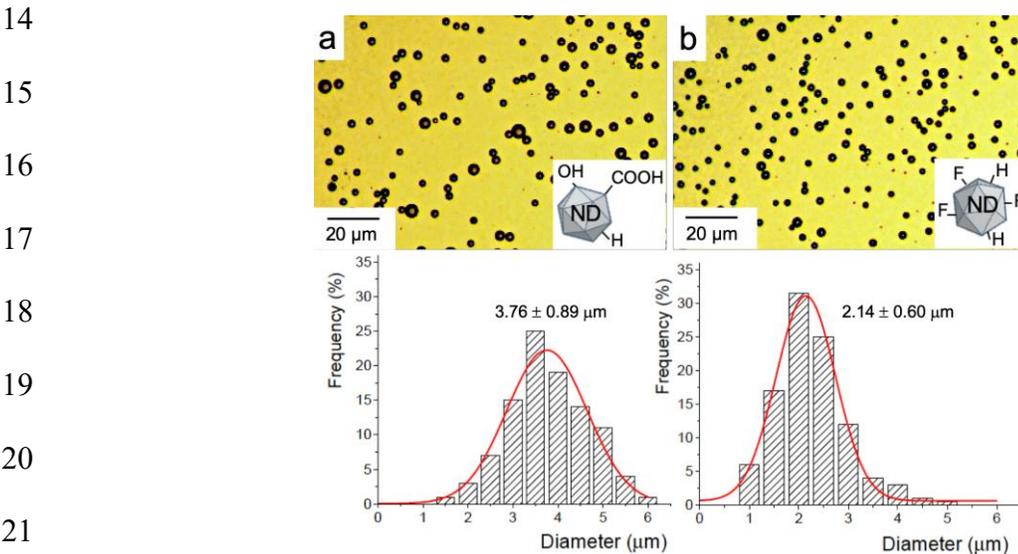
Figure 3. Optical micrographs of *F*-hexane-stabilized microbubbles shelled with a) ND25 and b) *F*-ND25, with corresponding size distributions. Concentration: 0.1 g L^{-1}; pH 12.0.
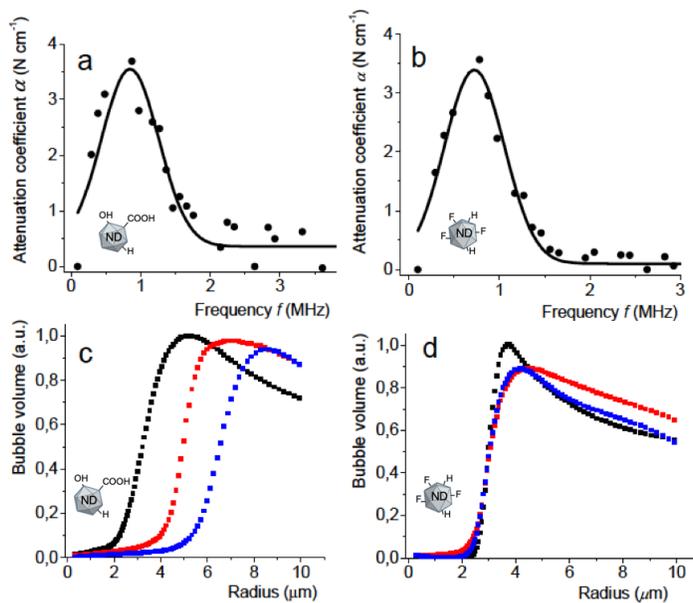
Figure 4. Variation of the attenuation coefficient α as a function of ultrasound frequency f for microbubbles prepared with dispersions of a) ND25 and b) F-ND25 under F-hexane. Size distributions of MBs shelled with c) ND25 and d) F-ND25 as measured acoustically after 5 (black), 10 (red) and 15 (blue) min.

The dependence of the MB volume fraction with size is plotted in Figure 4c,d for different time points. The distribution of ND25-shelled MBs is shifted toward larger radius values over time. By contrast, the mean radius of the fluorinated F-ND25-shelled MBs remains constant over time for at least 15 min. A hypothesis for the difference in the size distribution evolution is that F-ND25 are attracted to, and immobilized at the air/water interface through fluorine-fluorine interactions with supernatant F-hexane molecules. This is supported by the increased adsorption of F-ND25 upon F-hexane exposure, as monitored by tensiometry. It is also in line with previous data showing that iron oxide nanoparticles fitted with fluorinated group-terminated dendrons provided efficient stabilization of F-hexane-saturated air MBs.[45] The variation of the acoustically determined MB volume fraction plotted as a function of time allowed determination of the MB half-lives, which were ~15 min (SI Figure S3).

Altogether, these data show that ND-shelled MBs with small mean size can be generated owing to the presence of the *F*C gas. These MBs present echogenic properties that qualify them as a contrast agent for ultrasound diagnostics. More generally, the unique potential of NDs for sensing, bioimaging and drug delivery can be combined to the portfolio of applications of MBs in medicine and biology.

CONCLUSIONS AND PERSPECTIVES

In summary, exposure to a supernatant fluorocarbon gas strongly impacts, and in multiple ways, the behavior of aqueous dispersions of two types of nanodiamonds with different surface chemistry, nanodiamonds with a relatively polar surface, and more hydrophobic ones with a fluorinated surface. First, the *F*C effectively disaggregates the clusters that form spontaneously for both types of NDs. This helps surmount a critical, recurrent obstacle in nanodiamond implementation. As compared to other techniques of ND disaggregation, our method does not require dry (or wet) milling or prolonged tip sonication, processes that often produce contaminants that need to be removed by additional purification step. Second, the introduction of a supernatant *F*C gas strongly promotes the adsorption/recruitment of both types of NDs to the gas/water interface. Third, the fluorinated NDs experience increased adsorption relative to the non-fluorinated ones, revealing hydrophobic interactions with the *F*C. Fourth, ND-shelled microbubbles can be generated *only* when the *F*C is present, and this for both types of NDs, the fluorinated NDs leading to smaller MBs. Generation of microbubbles shelled with nanodiamonds is enabled by the *F*C gas that allows disaggregation of ND clusters in aqueous solution, and thus facilitates their diffusion to, and organization at the interface. Shorter, more water-soluble *F*Cs deserve investigation in order to enhance the disaggregating effect vis-à-vis other types of NDs (*e.g.* detonation NDs). Our data support a novel means of controlling nanodiamond aggregation,

22

as well as a novel approach to stabilize nanodiamond-shelled microbubbles, allowing investigation

of their potential as agents for bimodal contrast for ultrasound/fluorescence imaging, and drug

delivery. We believe that these findings open new perspectives and trigger new research, both

fundamental and mechanistic, and promote new applications in bioimaging and cell tracking.

ASSOCIATED CONTENT

Supporting Information. multinuclear solid-state NMR spectra, disaggregation induced by

perfluoropentane as monitored by DLS, and nanodiamond-shelled microbubble half-life (PDF).

AUTHOR INFORMATION

Corresponding Author* E-mail: krafft@unistra.fr, ORCID: ID: orcid.org/0000-0002-3379-2783

Author Contributions. The manuscript was written through contributions of all authors. All authors

have given approval to the final version of the manuscript.

The authors declare no competing financial interest.

REFERENCES

(1) Krueger, A. Diamond nanoparticles: Jewels for chemistry and physics. *Adv. Mater.* **2008,** *20*,

2445–2449.

(2) Mochalin, V. N.; Shenderova, O.; Ho, D.; Gogotsi, Y. The properties and applications of nanodiamonds. *Nat. Nanotechnol.* **2011** *7*,11-23.

(3) Nunn, N.; Torelli, M.; McGuire, G.; Shenderova, O. Nanodiamond: a high impact nanomaterial. *Curr. Opin. Solid State Mater. Sci.* **2017,** *21*, 1-9.

(4) Reina, G.; Zhao, L.; Bianco, A.; Komatsu, N. Chemical functionalization of nanodiamonds: opportunities and challenges ahead. *Angew. Chem. Int. Ed.* **2019,** *58*, 17918-17929.

(5) McGuinness, L. P.; Yan, Y.; Stacey, A.; Simpson, D. A.; Hall, L. T.; Maclaurin, D.; Prawer, S.; Mulvaney, P.; Wrachtrup, J.; Caruso, F.; Scholten, R. E.; Hollenberg, L. C. L. Quantum measurement and orientation tracking of fluorescent nanodiamonds inside living cells. *Nat. Nanotechnol.* **2011,** *6*, 358-363.

(6) Zhu, Y.; Li, J.; Li, W.; Zhang, Y.; Yang, X.; Chen, N.; Sun, Y.; Zhao, Y.; Fan, C.; Huang, Q. The biocompatibility of nanodiamonds and their application in drug delivery systems. *Theranostics* **2012,** *2*, 302.

(7) Happel, P.; Waag, T.; Schimke, M.; Schweeberg, S.; Muzha, A.; Fortak, K.; Heesch, D.; Klask, L.; Pilscheur, M.; Hoppe, F.; Lenders, T.; Meijer, J.; Lepperdinger, G.; Krueger, A. Intrinsically 32P-labeled diamond nanoparticles for in vivo imaging and quantification of their biodistribution in chicken embryos. *Adv. Funct. Mater.* **2018,** *28*, 1802873.

(8) Montalti, M.; Cantelli, A.; Battistelli, G. Nanodiamonds and silicon quantum dots: ultrastable and biocompatible luminescent nanoprobes for long-term bioimaging. *Chem. Soc. Rev.* **2015,** *44*, 4853-921.

(9) Shenderova, O.; Nunn, N. Production and purification of nanodiamonds. In *Nanodiamonds: Advanced Materials, Analysis, Properties and Applications*; Arnault, J. C., Ed.; Elsevier: Amsterdam, 2017; Chapter 2, pp 25-56.

1 (10) Krüger, A.; Kataoka, F.; Ozawa, M.; Fujino, T.; Suzuki, Y.; Aleksenskii, A. E.; Vul, A. Y.;

2 Osawa, E. Unusually tight aggregation in detonation nanodiamond: identification and

3 disintegration. *Carbon* **2005,** *43*, 1722-1730.

4 (11) Pentecost, A.; Gour, S.; Mochalin, V.; Knoke, I.; Gogotsi, Y. Deaggregation of nanodiamond

5 powders using salt- and sugar-assisted milling. *ACS Appl. Mater. Interfaces* **2010,** *2*, 3289–3294.

6 (12) Liang, Y.; Ozawa, M.; Krueger, A. A general procedure to functionalize agglomerating

7 nanoparticles demonstrated on nanodiamond. *ACS Nano* **2009,** *3*, 2288–2296.

8 (13) Ozawa, M.; Inaguma, M.; M.Takahashi; Kataoka, F.; Krüger, A.; Osawa, E. Preparation and

9 behavior of brownish, clear nanodiamond colloids. *Adv. Mater.* **2007,** *19*, 1201–1206.

10 (14) Pedroso-Santana, S.; Sarabia-Saínz, A.; Fleitas-Salazar, N.; Santacruz-Gómez, K.; Acosta-

11 Elías, M.; Pedroza-Montero, M.; Riera, R. Deagglomeration and characterization of detonation

12 nanodiamonds for biomedical applications. *J. App. Biomed.* **2017,** *15*, 15-21.

13 (15) Turcheniuk, K.; Trecazzi, C.; Deeleepojananan, C.; Mochalin, V. N. Salt-assisted ultrasonic

14 deaggregation of nanodiamond. *ACS Appl. Mater. Interfaces* **2016,** *8*, 25461−25468.

15 (16) Betts, J. N.; Johnson, M. G.; Rygiewics, P. T.; King, G. A.; Andersen, C. P. Potential for

16 metal contamination by direct sonication of nanoparticle suspension. *Environ. Toxicol. Chem.*

17 **2013,** *32*, 889–893.

18 (17) Merz, V.; Lenhart, J.; Vonhausen, Y.; Ortiz-Soto, M. E.; Seibel, J.; Krueger, A. Zwitterion-

19 functionalized detonation nanodiamond with superior protein repulsion and colloidal stability in

20 physiological media. *Small* **2019,** *15*, 1901551.

21 (18) Tiainen, T.; Myllymäki, T. T. T.; Hatanpää, T.; Tenhu, H.; Hietala, S. Polyelectrolyte

22 stabilized nanodiamond dispersions. *Diam. Relat. Mater.* **2019,** *95*, 185-194.

(19) Wang, T.; Handschuh-Wang, S.; Qin, P.; Yang, Y.; Zhou, X.; Tang, Y. Enhancing the colloidal stability of detonation synthesized diamond particles in aqueous solutions by adsorbing organic mono-, bi- and tridentate molecules. *J. Colloid Interface Sci.* **2017,** *499*, 102-109.

(20) Sotoma, S.; Hsieh, F. J.; Chen, Y.-W.; Tsai, P.-C.; Chang, H.-C. Highly stable lipid-encapsulation of fluorescent nanodiamonds for bioimaging applications. *Chem. Commun.* **2018,** *54*, 1000-1003.

(21) Bumb, A.; Sarkar, S. K.; Billington, N.; Brechbiel, M. W.; Neuman, K. C. Silica encapsulation of fluorescent nanodiamonds for colloidal stability and facile surface functionalization. *J. Am. Chem. Soc.* **2017,** *135*, 7815−7818.

(22) Jung, H.-S.; Cho, K.-J.; Seol, Y.; Takagi, Y.; Dittmore, A.; Roche, P. A.; Neuman, K. C. Polydopamine encapsulation of fluorescent nanodiamonds for biomedical applications. *Adv. Funct. Mater.* **2018,** *28*, 1801252.

(23) Schutt, E. S.; Klein, D. H.; Mattrey, R. M.; Riess, J. G. Injectable microbubbles as contrast agents for diagnostic ultrasound imaging: The key role of perfluorochemicals. *Angew. Chem. Int. Ed.* **2003,** *42*, 3218-3235.

(24) Kooiman, K.; Vos, H. J.; Versluis, M.; de Jong, N. Acoustic behavior of microbubbles and implications for drug delivery. *Adv. Drug Deliv. Rev.* **2014,** *72*, 28-48.

(25) Wang, S.; Hossack, J.; Klibanov, A. L. Targeting of microbubbles: contrast agents for ultrasound molecular imaging. *J. Drug Target.* **2018,** *26*, 420-434.

(26) Chong, W. K.; Papadopoulou, V.; Dayton, P. A. Imaging with ultrasound contrast agents: current status and future. *Abdom. Radiol.* **2018,** *43*, 762–772.

(27) Stride, E.; Segers, T.; Lajoinie, G.; Cherkaoui, S.; Bettinger, T.; Versluis, M.; Borden, M. Microbubble agents: New directions. *Ultrasound Med. Biol.* **2020,** *46*, 1326-1343.

(28) Kooiman, K.; Roovers, S.; Langeveld, S. A. G.; Kleven, R. T.; Dewitte, H.; O'Reilly, M. A.; Escoffre, J.-M.; Bouakaz, A.; Verweij, M. D.; Hynynen, K.; Lentacker, I.; Stride, E.; Holland, C. K. Ultrasound-responsive cavitation nuclei for therapy and drug delivery. *Ultrasound Med. Biol.* **2020,** *46*, 1296-1325.

(29) Fu, L.; Ke, H.-T. Nanomaterials incorporated ultrasound contrast agents for cancer theranostics. *Cancer Biol. Med.* **2016,** *13*, 313-324.

(30) Jamburidze, A.; Huerre, A.; Baresch, D.; Poulichet, V.; Corato, M. d.; Garbin, V. Nanoparticle-coated microbubbles for combined ultrasound imaging and drug delivery. *Langmuir* **2019,** *35*, 10087−10096.

(31) Yang, G.; O'Duill, M.; Gouverneur, V.; Krafft, M. P. Recruitment and immobilization of a fluorinated biomarker across an interfacial phospholipid film using a fluorocarbon gas. *Angew. Chem. Int. Ed.* **2015,** *54*, 8402-8406.

(32) Gazzera, L.; Milani, R.; Pirrie, L.; Schmutz, M.; Blanck, C.; Resnati, G.; Metrangolo, P.; Krafft, M. P. Design of highly stable echogenic microbubbles through controlled assembly of their hydrophobin shell. *Angew. Chem. Int. Ed.* **2016,** *55*, 10263-10267.

(33) Ando, Y.; H. Tabata; Sanchez, M.; Cagna, A.; Koyama, D.; Krafft, M. P. Microbubbles with a self-assembled poloxamer shell and a fluorocarbon inner gas. *Langmuir* **2016,** *32*, 12461-12467.

(34) Garbin, V.; Crocker, J. C.; Stebe, K. J. Nanoparticles at fluid interfaces: Exploiting capping ligands to control adsorption, stability and dynamics. *J. Colloid Interface Sci.* **2012,** *387*, 1-11.

(35) Dubois, M.; Guérin, K.; Batisse, N.; Petit, E.; Hamwi, A.; Komatsu, N.; Kharbache, H.; Pirotte, P.; Masin, F. Solid state NMR study of nanodiamond surface chemistry. *Solid State Nucl. Magn. Reson.* **2011,** *40*, 144-154.

1 (36) Zagrebina, E. M.; Generalov, A. V.; Klyushin, A. Y.; Simonov, K. A.; Vinogradov, N. A.;

2 Dubois, M.; Frezet, L.; Mårtensson, N.; Preobrajenski, A. B.; Vinogradov, A. S. Comparative

3 NEXAFS, NMR, and FTIR study of various-sized nanodiamonds: As-prepared and fluorinated. *J.*

4 *Phys. Chem. C* **2015,** *119*, 835−844.

5 (37) Szijjarto, C.; Rossi, S.; Waton, G.; Krafft, M. P. Effects of perfluorocarbon gases on the size

6 and stability characteristics of phospholipid-coated microbubbles - Osmotic effect versus

7 interfacial film stabilization. *Langmuir* **2012,** *28*, 1182-1189.

8 (38) Hassan, P. A.; Rana, S.; Verma, G. Making sense of Brownian motion: Colloid

9 characterization by dynamic light scattering. *Langmuir* **2014,** *31*, 3−12.

10 (39) Nguyen, P. N.; Veschgini, M.; Tanaka, M.; Waton, G.; Vandamme, T.; Krafft, M. P.

11 Counteracting the inhibitory effect of proteins towards lung surfactant substitutes: a fluorocarbon

12 gas helps displace albumin at the air/water interface. *Chem. Commun.* **2014,** *50*, 11576-11579.

13 (40) Rossi, S.; Waton, G.; Krafft, M. P. Phospholipid-coated gas bubble engineering - Key

14 parameters for size and stability control as determined by an acoustic method. *Langmuir* **2010,** *26*,

15 1649-1655.

16 (41) Kabalnov, A.; Klein, D.; Pelura, T.; Schutt, E.; Weers, J. Dissolution of multicomponent

17 microbubbles in the blood stream: 1. Theory. *Ultrasound Med. Biol.* **1998,** *24*, 739-749.

18 (42) Gibson, N.; Shenderova, O.; Luo, T. J. M.; Moseenkov, S.; Bondar, V.; Puzyr, A.; Purtov, K.;

19 Fitzgerald, Z.; Brenner, D. W. Colloidal stability of modified nanodiamond particles. *Diam. Relat.*

20 *Mater.* **2009,** *18*, 620–626.

21 (43) Xu, X.; Yu, Z.; Zhu, Y.; Wang, B. Effect of sodium oleate adsorption on the colloidal stability

22 and zeta potential of detonation synthesized diamond particles in aqueous solutions. *Diamond*

23 *Relat. Mater.* **2005,** *14*, 206-212.

1 (44) Machida, H.; Ohashi, T.; Akasaka, S.; Fujimori, A. Formation of organized films with

2 fluorocarbon-modified inorganic nanoparticles and their nanodispersion behavior in solvent. *J.*

3 *Fluorine Chem.* **2020,** *230*, 109433.

4 (45) Shi, D.; Wallyn, J.; Nguyen, D.-V.; Perton, F.; Felder-Flesch, D.; Bégin-Colin, S.; Maaloum,

5 M.; Krafft, M. P. Microbubbles decorated with dendronized magnetic nanoparticles for biomedical

6 imaging. Effective stabilization via fluorous interactions. *Beilstein J. Nanotechnol.* **2019,** *10*, 2103-

7 2115.

8 (46) Shi, D.; Liu, X.; Counil, C.; Krafft, M. P. Fluorocarbon exposure mode markedly affects

9 phospholipid monolayer behavior at the gas/liquid interface: Impact on size and stability of

10 microbubbles. *Langmuir* **2019,** *35*, 10025-10033..

11 (47) Kwan, J. J.; Borden, M. A. Lipid monolayer collapse and microbubble stability. *Adv. Coll.*

12 *Interface Sci.* **2012,** *183-184*, 82-99.

13